Frequency-domain online modeling of multiple secondary paths without auxiliary noise for active noise control

Siyuan Lian*, Xiaofeng Zeng*, Ruquan Sun* and Jing Lu†
Key Laboratory of Modern Acoustics, Institute of Acoustics, Nanjing University, Nanjing, China
* E-mail: {siyuan.lian, xiaofeng.zeng, ruquan.sun}@smail.nju.edu.cn
† E-mail: lujing@nju.edu.cn

***Abstract*—Accurate secondary path modeling is critical for the stability and effectiveness of active noise control systems. While offline secondary path modeling yields precise estimates before system control, it fails to accommodate time-varying environments. Online methods utilizing auxiliary noise enhance adaptability but inevitably increase residual noise. Neural network-based approaches offer data-driven alternatives; however, they demand substantial computational resources and prior training. Building upon prior single-channel work, this paper proposes a frequency-domain online modeling algorithm for multiple secondary paths without auxiliary noise. Theoretical analysis confirms the uniqueness of the modeling paths and control filters, and the frequency-domain processing substantially reduces computational complexity compared to the existing online modeling algorithm. Simulations in a multichannel ANC system demonstrate that the proposed algorithm achieves fast convergence and superior tracking performance under acoustic path variations, demonstrating its suitability for real-time applications in dynamic scenarios.**

I. Introduction

Active noise control (ANC) effectively mitigates low-frequency noise by generating anti-noise signals that destructively interfere with the primary noise [1, 2]. The effectiveness and stability of ANC systems, especially in feedforward multichannel configurations, heavily rely on the accurate modeling of the secondary path—the acoustic transfer function from the secondary source to the error microphone [3]. Traditionally, this modeling is performed offline prior to the control process. However, fixed models fail to cope with time-varying acoustic environments induced by temperature shifts, physical movements, or structural changes [4]. This necessitates online secondary path modeling, enabling the simultaneous execution of secondary path estimation and ANC.

A classical approach for online secondary path modeling is to inject low-level auxiliary noise into the control signal to continuously identify the secondary path [5-7]. However, this injected noise inevitably adds to the residual error and can deteriorate the noise reduction performance. Moreover, in multichannel systems with multiple paths to model, the cumulative effect of auxiliary noise becomes more pronounced [8].

In parallel, neural network-based approaches have also been investigated for secondary path modeling due to their strong nonlinear mapping capability [4]. Deep neural networks demonstrate promise in modeling complex and time-varying acoustic responses [4, 9]. However, these methods often require extensive offline training, large datasets, and significant computational resources, limiting their practicality in real-time ANC applications.

Recent efforts have explored auxiliary-noise-free approaches that reuse the control signal as the excitation for modeling. These methods exploit the inherent excitation in the control signal to estimate the secondary path adaptively, thereby eliminating the need for additional noise [10]. For example, Hu *et al*. proposed an online time-domain modeling approach for multichannel ANC without auxiliary noise, achieving stable convergence under moderate dynamics [11]. However, it entails high computational complexity and lacks explicit analysis of the convergence behavior of the control filters.

Frequency-domain implementations significantly reduce computational complexity by leveraging fast Fourier transform (FFT) and block processing technique [12, 13]. In this paper, a frequency-domain online modeling algorithm is proposed for multiple secondary paths without auxiliary noise, which is named as frequency-domain synchronous control and modeling (FDSCM) algorithm. The algorithm updates the control and path modeling filters based on frequency-domain filtered-reference normalized least mean square (FDFxNLMS) algorithm to alleviate computational burden and accelerate the convergence speed. Theoretical analysis proves the uniqueness of the modeling paths and control filters, and simulations validate the algorithm's performance in terms of faster convergence, lower computational cost, and enhanced tracking

979-8-3315-7206-8/25/$31.00

capability in a 1 × 2 × 2 multichannel ANC system.

II. Online Modeling of Multiple Secondary Paths without Auxiliary Noise

The 1 × *C* × *M* online secondary path modeling ANC system integrates one reference signal, *C* control signals emitted by secondary sources, and *M* error signals captured by the error microphones. The lengths of the control filters, secondary paths and primary paths are denoted as *I*, *J* and *K*, respectively. By leveraging control filter outputs for secondary path estimation, this multichannel architecture enables concurrent path identification and noise cancellation. The modeling process with respect to the *m*-th error microphone at time *n* is illustrated in Fig. 1.

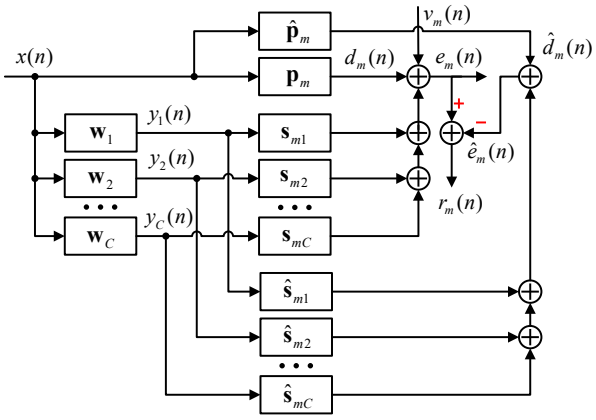

Fig.1. The modeling process with respect to the *m*-th error microphone.

Reference signal $x(n)$ propagates through the m-th primary path vector $\mathbf{p}_m = [p_{m,0}\ p_{m,1}\ \cdots\ p_{m,K-1}]^{\mathrm{T}}$, producing the desired signal $d_{\mathrm{m}}(n)$:

$$d_m(n) = \mathbf{p}_m^{\mathrm{T}}\mathbf{x}_{\mathbf{p}}(n) + v_m(n), \tag{1}$$

where the superscript $^{\mathrm{T}}$ signifies the transpose operation, $\mathbf{x}_{\mathbf{p}}(n) = [x(n)\ x(n-1)\ \cdots\ x(n-K+1)]^{\mathrm{T}}$ is the reference signal vector for primary paths, and $v_m(n)$ represents the uncorrelated system noise. Simultaneously, the c-th control signal is generated by filtering the reference signal through the control filter vector $\mathbf{w}_c = [w_{c,0}\ w_{c,1}\ \cdots\ w_{c,I-1}]^{\mathrm{T}}$:

$$y_c(n) = \mathbf{w}_c^{\mathrm{T}}\mathbf{x}_{\mathbf{w}}(n), \tag{2}$$

where $\mathbf{x}_{\mathbf{w}}(n) = [x(n)\ x(n-1)\ \cdots\ x(n-I+1)]^{\mathrm{T}}$ denotes the reference signal vector for control filters. Subsequently, these control signals traverse the secondary paths and destructively interfere with the desired signal $d_{\mathrm{m}}(n)$ at the m-th error microphone, yielding the error signal:

$$e_m(n) = d_m(n) + \sum_{c=1}^{C}\mathbf{s}_{mc}^{\mathrm{T}}\mathbf{y}_c(n), \tag{3}$$

where $\mathbf{s}_{mc} = [s_{mc,0}\ s_{mc,1}\ \cdots\ s_{mc,J-1}]^{\mathrm{T}}$ denotes the secondary path vector from the c-th secondary source to the m-th error microphone, and $\mathbf{y}_c(n) = [y_c(n)\ y_c(n-1)\ \cdots\ y_c(n-J+1)]^{\mathrm{T}}$ is the c-th control signal vector. Replacing (2) in (3) yields

$$e_m(n) = d_m(n) + \mathbf{s}_m^{\mathrm{T}}\bar{\mathbf{U}}(n)\mathbf{w}, \tag{4}$$

where $\mathbf{s}_m = [\mathbf{s}_{m1}^{\mathrm{T}}\ \cdots\ \mathbf{s}_{mC}^{\mathrm{T}}]^{\mathrm{T}} \in \mathcal{R}^{CJ\times 1}$, $\mathbf{w} = [\mathbf{w}_1^{\mathrm{T}}\ \cdots\ \mathbf{w}_C^{\mathrm{T}}]^{\mathrm{T}} \in \mathcal{R}^{CI\times 1}$, and $\bar{\mathbf{U}}(n) = \begin{bmatrix}\mathbf{U}(n) & \cdots & \mathbf{0}_{J\times I}\\ \vdots & \ddots & \vdots\\ \mathbf{0}_{J\times I} & \cdots & \mathbf{U}(n)\end{bmatrix} \in \mathcal{R}^{CJ\times CI}$ with $\mathbf{0}_{a\times b}$ denoting an $a \times b$ zero matrix. The reference signal matrix $\mathbf{U}(n)$ is given by

$$\mathbf{U}(n) = \begin{bmatrix}\mathbf{x}_{\mathbf{w}}^{\mathrm{T}}(n)\\ \mathbf{x}_{\mathbf{w}}^{\mathrm{T}}(n-1)\\ \vdots\\ \mathbf{x}_{\mathbf{w}}^{\mathrm{T}}(n-J+1)\end{bmatrix} \in \mathcal{R}^{J\times I}. \tag{5}$$

Defining the primary and secondary path modeling filters as $\hat{\mathbf{p}}_m = [\hat{p}_{m,0}\ \cdots\ \hat{p}_{m,K-1}]^{\mathrm{T}}$ and $\hat{\mathbf{s}}_{mc} = [\hat{s}_{mc,0}\ \cdots\ \hat{s}_{mc,J-1}]^{\mathrm{T}}$, the estimated desired signal can be expressed similarly to (1) as

$$\hat{d}_m(n) = \hat{\mathbf{p}}_m^{\mathrm{T}}\mathbf{x}_{\mathbf{p}}(n), \tag{6}$$

while the estimated error signal can be expressed similarly to (4) as

$$\hat{e}_m(n) = \hat{d}_m(n) + \hat{\mathbf{s}}_m^{\mathrm{T}}\bar{\mathbf{U}}(n)\mathbf{w}. \tag{7}$$

Subtracting (7) from (4) results in the modeling error signal:

$$r_m(n) = (\mathbf{p}_m^{\mathrm{T}} - \hat{\mathbf{p}}_m^{\mathrm{T}})\mathbf{x}_{\mathbf{p}}(n) + (\mathbf{s}_m^{\mathrm{T}} - \hat{\mathbf{s}}_m^{\mathrm{T}})\bar{\mathbf{U}}(n)\mathbf{w} + v_m(n). \tag{8}$$

III. Frequency-Domain Synchronous Control and Modeling Algorithm

A. Frequency-domain Implementation

In this paper, the control filters and acoustic path modeling filters are updated in the frequency domain based on the normalized least mean square algorithm, as illustrated in Fig. 2. The 50% overlap-save method is employed [1, 12], where the lengths of the control filter (I), the secondary path modeling filter (J) and the primary path modeling filter (K) are all set equal to the block length L, i.e., $I = J = K = L$, to facilitate efficient implementation for the 2L-point FFT.

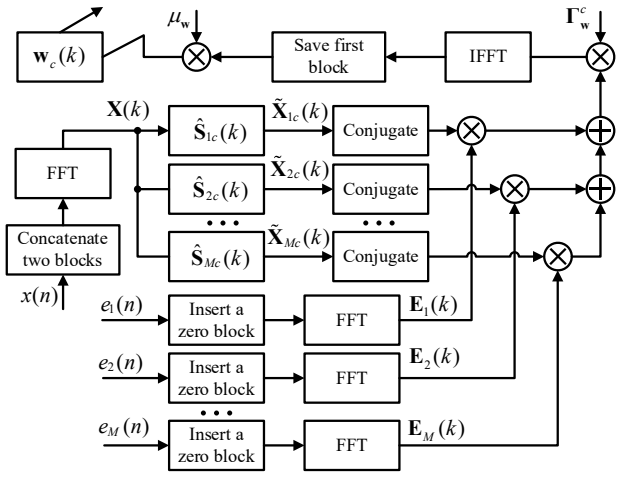

(a)

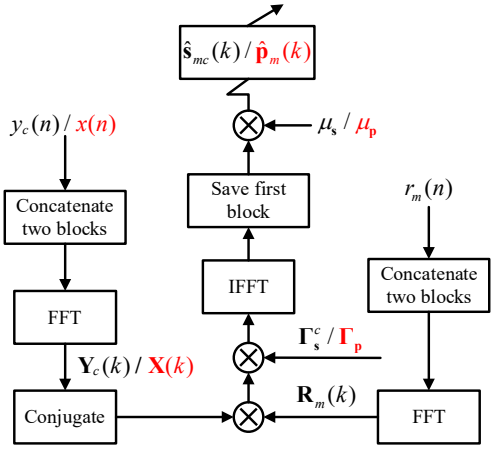

(b)

Fig. 2. The block diagrams for updating (a) the control filter and (b) the acoustic path modeling filter.

At the k-th iteration, the latest block of the reference signal is padded with the previous block to form a $2L$-tap vector: $\mathbf{x}(k) = [x(kL-L)\ \cdots\ x(kL-1)\ x(kL)\ \cdots\ x(kL+L-1)]^{\mathrm{T}}$. With $\mathbf{F}$ and $\mathbf{F}^{-1}$ denoting the discrete Fourier transform (DFT) matrix and inverse DFT matrix [12, 14], the corresponding frequency-domain block can be described as

$$\mathbf{X}(k) = diag\{\mathbf{F}\mathbf{x}(k)\} \in \mathcal{R}^{2L\times 2L}, \tag{9}$$

where $diag\{\bullet\}$ constructs a diagonal matrix from its input along the diagonal [15]. Subsequently, the filtered-reference signal block is represented as

$$\tilde{\mathbf{X}}_{mc}(k) = diag\{\mathbf{X}(k)\hat{\mathbf{S}}_{mc}(k)\}, \tag{10}$$

where $\hat{\mathbf{S}}_{mc}(k) = \mathbf{F}[\hat{\mathbf{s}}_{mc}^{\mathrm{T}}(k), \mathbf{0}_{1\times L}]^{\mathrm{T}}$ is the frequency-domain response of the mc-th secondary path modeling filter at the k-th iteration.

After padding the new error signal block $\mathbf{e}_m(k) = [e_m(kL)\ e_m(kL+1)\ \cdots\ e_m(kL+L-1)]^{\mathrm{T}}$ with a block of zeros, the frequency-domain error signal vector $\mathbf{E}_{\mathbf{w}}(k)$ is calculated as

$$\mathbf{E}_m(k) = \mathbf{F}[\mathbf{0}_{1\times L}\ \mathbf{e}_m^{\mathrm{T}}(k)]^{\mathrm{T}} = \mathbf{F}\mathbf{Q}_{L1}^{\mathrm{T}}\mathbf{e}_m(k), \tag{11}$$

with $\mathbf{Q}_{L1} = [\mathbf{0}_{L\times L}\ \mathbf{I}_L]$. Based on FDFxNLMS algorithm, the update equation of the c-th control filter is expressed as [16]:

$$\mathbf{w}_c(k+1) = \mathbf{w}_c(k) - \mu_{\mathbf{w}}\mathbf{Q}_{1L}\mathbf{F}^{-1}\mathbf{\Gamma}_{\mathbf{w}}^c\sum_{m=1}^{M}[\tilde{\mathbf{X}}_{mc}^{\mathrm{H}}(k)\mathbf{E}_m(k)], \tag{12}$$

where $\mu_{\mathbf{w}}$ is the step size of the control filter, the superscript $^{\mathrm{H}}$ is the conjugate transpose and $\mathbf{Q}_{1L} = [\mathbf{I}_L\ \mathbf{0}_{L\times L}]$. $\mathbf{\Gamma}_{\mathbf{w}}^c = \{\sum_{m=1}^{M}\mathbb{E}\{\tilde{\mathbf{X}}_{mc}^{\mathrm{H}}(k)\tilde{\mathbf{X}}_{mc}(k)\}\}^{-1}$ represents the reciprocal of the filtered-reference signal power spectrum to accelerate the convergence [13].

As illustrated in Fig. 2(b), the update equations of the secondary and primary path modeling filters can be derived in a similar form to (12):

$$\begin{aligned}\mathbf{s}_{mc}(k+1) &= \mathbf{s}_{mc}(k) + \mu_{\mathbf{s}}\mathbf{Q}_{1L}\mathbf{F}^{-1}\mathbf{\Gamma}_{\mathbf{s}}^c\mathbf{Y}_c^{\mathrm{H}}(k)\mathbf{R}_m(k),\\ \mathbf{p}_m(k+1) &= \mathbf{p}_m(k) + \mu_{\mathbf{p}}\mathbf{Q}_{1L}\mathbf{F}^{-1}\mathbf{\Gamma}_{\mathbf{p}}\mathbf{X}^{\mathrm{H}}(k)\mathbf{R}_m(k),\end{aligned} \tag{13}$$

where $\mu_{\mathbf{s}}$ and $\mu_{\mathbf{p}}$ are the step sizes of the secondary and primary path modeling filters, respectively. $\mathbf{R}_m(k) = \mathbf{F}[\mathbf{0}_{1\times L}\ \mathbf{r}_m^{\mathrm{T}}(k)]^{\mathrm{T}} = \mathbf{F}\mathbf{Q}_{L1}^{\mathrm{T}}\mathbf{r}_m(k)$ is the frequency-domain modeling error signal vector with $\mathbf{r}_m(k) = [r_m(kL)\ r_m(kL+1)\ \cdots\ r_m(kL+L-1)]^{\mathrm{T}}$. The normalized factors in (13) are calculated as

$$\begin{aligned}\mathbf{\Gamma}_{\mathbf{s}}^c &= \{\mathbb{E}\{\mathbf{Y}_c^{\mathrm{H}}(k)\mathbf{Y}_c(k)\}\}^{-1},\\ \mathbf{\Gamma}_{\mathbf{p}} &= \{\mathbb{E}\{\mathbf{X}^{\mathrm{H}}(k)\mathbf{X}(k)\}\}^{-1},\end{aligned} \tag{14}$$

where $\mathbf{Y}_c(k) = diag\{\mathbf{F}\mathbf{y}_c(k)\}$ and $\mathbf{y}_c(k) = [y_c(kL-L)\ \cdots\ y_c(kL-1)\ y_c(kL)\ \cdots\ y_c(kL+L-1)]^{\mathrm{T}}$.

B. Convergence Analysis

To facilitate a unified representation of the reference signals in (8), a consolidated reference signal vector is defined as $\mathbf{x}(n) = [x(n)\ x(n-1)\ \cdots\ x(n-G+1)]^{\mathrm{T}}$, where $G \geq \max(I+J-1, K)$. Substituting this vector into (8) yields

$$r_m(n) = (\mathbf{p}_m^{\mathrm{T}} - \hat{\mathbf{p}}_m^{\mathrm{T}})\mathbf{A}_1\mathbf{x}(n) + (\mathbf{s}_m^{\mathrm{T}} - \hat{\mathbf{s}}_m^{\mathrm{T}})\mathbf{W}\mathbf{A}_2\mathbf{x}(n) + v_m(n), \tag{15}$$

where $\mathbf{A}_1 = [\mathbf{I}_K\ \mathbf{0}_{K\times(G-K)}] \in \mathcal{R}^{K\times G}$ with $\mathbf{I}_g$ representing $g \times g$ identity matrix, and $\mathbf{A}_2 = [\mathbf{I}_{I+J-1}\ \mathbf{0}_{(I+J-1)\times(G-I-J+1)}] \in \mathcal{R}^{(I+J-1)\times G}$. $\mathbf{W} = [\mathbf{W}_1^{\mathrm{T}}\ \cdots\ \mathbf{W}_C^{\mathrm{T}}]^{\mathrm{T}} \in \mathcal{R}^{CJ\times(I+J-1)}$ and

$$\mathbf{W}_c = \left[\begin{array}{cccc:ccc} w_{c,0} & w_{c,1} & \cdots & w_{c,I-1} & 0 & \cdots & 0\\ 0 & w_{c,0} & w_{c,1} & \cdots & w_{c,I-1} & \ddots & \vdots\\ \vdots & 0 & \ddots & \cdots & \cdots & \ddots & 0\\ 0 & \cdots & 0 & w_{c,0} & w_{c,1} & \cdots & w_{c,I-1}\end{array}\right]. \tag{16}$$

Subsequently, the mean square error (MSE) [8] of (15) is derived as

$$\zeta = \mathbb{E}\{r_m^2(n)\} = \mathbf{\theta}_m^{\mathrm{T}}\mathbb{E}\{\mathbf{x}(n)\mathbf{x}^{\mathrm{T}}(n)\}\mathbf{\theta}_m + \sigma_{v_m}^2, \tag{17}$$

where $\mathbb{E}\{\bullet\}$ is the expectation operator, $\sigma_{v_m}^2 = \mathbb{E}\{v_m^2(n)\}$ and

$$\mathbf{\theta}_m = \mathbf{A}_1^{\mathrm{T}}(\mathbf{p}_m - \hat{\mathbf{p}}_m) + \mathbf{A}_2^{\mathrm{T}}\mathbf{W}^{\mathrm{T}}(\mathbf{s}_m - \hat{\mathbf{s}}_m). \tag{18}$$

As long as the control filter coefficients are none-zero and time-varying, Eq. (18) admits unique solutions for the modeling filters, specifically $\hat{\mathbf{p}}_m = \mathbf{p}_m$ and $\hat{\mathbf{s}}_m = \mathbf{s}_m$ [10, 11].

For control filters, the circular matrices can be diagonalized by DFT matrices [15] as

$$\begin{aligned}\mathbf{\Psi}_{\mathbf{w}}^c &= \mathbf{F}^{-1}\mathbf{\Gamma}_{\mathbf{w}}^c\mathbf{F} = \mathbf{F}^{-1}\{\sum_{m=1}^{M}\mathbb{E}\{\tilde{\mathbf{X}}_{mc}^{\mathrm{H}}(k)\tilde{\mathbf{X}}_{mc}(k)\}\}^{-1}\mathbf{F}\\ &= \begin{bmatrix}\mathbf{\Psi}_{\mathbf{w}1}^c & \mathbf{\Psi}_{\mathbf{w}2}^c\\ \mathbf{\Psi}_{\mathbf{w}2}^c & \mathbf{\Psi}_{\mathbf{w}1}^c\end{bmatrix},\end{aligned} \tag{19}$$

and

$$\mathbf{\Phi}_{\mathbf{w}}^{mc}(k) = \mathbf{F}^{-1}\tilde{\mathbf{X}}_{mc}^{\mathrm{H}}(k)\mathbf{F} = \begin{bmatrix}\mathbf{\Phi}_{\mathbf{w}1}^{mc}(k) & \mathbf{\Phi}_{\mathbf{w}2}^{mc}(k)\\ \mathbf{\Phi}_{\mathbf{w}2}^{mc}(k) & \mathbf{\Phi}_{\mathbf{w}1}^{mc}(k)\end{bmatrix}. \tag{20}$$

Substituting (19) and (20) into (12) yields

$$\begin{aligned}\mathbf{w}_c(k+1) &= \mathbf{w}_c(k) - \mu_{\mathbf{w}} \sum_{m=1}^{M} [\mathbf{Q}_{1L} \mathbf{F}^{-1} \boldsymbol{\Gamma}_{\mathbf{w}}^{c} \tilde{\mathbf{X}}_{mc}^{\mathrm{H}}(k) \mathbf{E}_m(k)] \\ &= \mathbf{w}_c(k) - \mu_{\mathbf{w}} \sum_{m=1}^{M} [\mathbf{Q}_{1L} \boldsymbol{\Psi}_{\mathbf{w}}^{c} \boldsymbol{\Phi}_{\mathbf{w}}^{mc}(k) \mathbf{Q}_{L1}^{\mathrm{T}} \mathbf{e}_m(k)] \\ &= \mathbf{w}_c(k) - \mu_{\mathbf{w}} \sum_{m=1}^{M} [\boldsymbol{\Omega}_{\mathbf{w}}^{mc}(k) \mathbf{e}_m(k)],\end{aligned} \tag{21}$$

with $\boldsymbol{\Omega}_{\mathbf{w}}^{mc}(k) = \boldsymbol{\Psi}_{\mathbf{w}1}^{c} \boldsymbol{\Phi}_{\mathbf{w}2}^{mc}(k) + \boldsymbol{\Psi}_{\mathbf{w}2}^{c} \boldsymbol{\Phi}_{\mathbf{w}1}^{mc}(k)$. If the steady-state solution of the c-th control filter is $\mathbf{w}_c^{\infty}$, the weight-error vector can be defined as

$$\tilde{\mathbf{w}}_c(k) = \mathbf{w}_c^{\infty} - \mathbf{w}_c(k), \tag{22}$$

and the desired signal block $\mathbf{d}_m(k) = [d_m(kL)\ d_m(kL+1) \cdots d_m(kL+L-1)]^{\mathrm{T}}$ can be obtained as

$$\mathbf{d}_m(k) = -\sum_{c=1}^{C} \boldsymbol{\Phi}_{\mathbf{w}2}^{mc}(k) \mathbf{w}_c^{\infty} + \mathbf{v}_m(k), \tag{23}$$

with $\mathbf{v}_m(k) = [v_m(kL)\ v_m(kL+1) \cdots v_m(kL+L-1)]^{\mathrm{T}}$. Substituting (22) into (21) yields

$$\tilde{\mathbf{w}}_c(k+1) = \tilde{\mathbf{w}}_c(k) + \mu_{\mathbf{w}} \sum_{m=1}^{M} [\boldsymbol{\Omega}_{\mathbf{w}}^{mc}(k) \mathbf{e}_m(k)]. \tag{24}$$

Rewriting $\mathbf{e}_m(k)$ as

$$\mathbf{e}_m(k) = \mathbf{d}_m(k) + \sum_{c=1}^{C} \boldsymbol{\Phi}_{\mathbf{w}2}^{mc}(k) \mathbf{w}_c(k), \tag{25}$$

and substituting (23) and (25) into (24) yields

$$\begin{aligned}\tilde{\mathbf{w}}_c(k+1) = \tilde{\mathbf{w}}_c(k) &- \mu_{\mathbf{w}} \sum_{m=1}^{M} \sum_{c'=1}^{C} \boldsymbol{\Omega}_{\mathbf{w}}^{mc}(k) \boldsymbol{\Phi}_{\mathbf{w}2}^{mc'}(k) \tilde{\mathbf{w}}_{c'}(k) \\ &+ \mu_{\mathbf{w}} \sum_{m=1}^{M} \boldsymbol{\Omega}^{mc}(k) \mathbf{v}_m(k)\end{aligned}. \tag{26}$$

Two assumptions are adopted for the mathematical tractability: (A1) All signals are zero-mean stationary processes with continuous spectra, and the system noise is i.i.d. and uncorrelated with the reference signals; (A2) The reference signals and the control filters are independent of each other. Taking expectation of both sides of (26) results in

$$\mathbb{E}\{\tilde{\mathbf{w}}_c(k+1)\} = \mathbb{E}\{\tilde{\mathbf{w}}_c(k)\} - \mu_{\mathbf{w}} \sum_{c'=1}^{C} \boldsymbol{\Lambda}_{cc'} \mathbb{E}\{\tilde{\mathbf{w}}_{c'}(k)\}, \tag{27}$$

where $\boldsymbol{\Lambda}_{cc'} = \sum_{m=1}^{M} \mathbb{E}\{\boldsymbol{\Omega}_{\mathbf{w}}^{mc}(k) \boldsymbol{\Phi}_{\mathbf{w}2}^{mc'}(k)\}$.

Defining the global weight-error expectation vector as $\mathbb{E}\{\tilde{\mathbf{w}}(k)\} = [\mathbb{E}\{\tilde{\mathbf{w}}_1^{\mathrm{T}}(k)\}\ \mathbb{E}\{\tilde{\mathbf{w}}_2^{\mathrm{T}}(k)\} \cdots \mathbb{E}\{\tilde{\mathbf{w}}_C^{\mathrm{T}}(k)\}]^{\mathrm{T}}$ yields

$$\mathbb{E}\{\tilde{\mathbf{w}}(k+1)\} = (\mathbf{I}_{CL} - \mu_{\mathbf{w}} \boldsymbol{\Lambda}) \mathbb{E}\{\tilde{\mathbf{w}}(k)\}, \tag{28}$$

where $\boldsymbol{\Lambda} = \begin{bmatrix} \boldsymbol{\Lambda}_{11} & \boldsymbol{\Lambda}_{12} & \cdots & \boldsymbol{\Lambda}_{1C} \\ \boldsymbol{\Lambda}_{21} & \ddots & \ddots & \boldsymbol{\Lambda}_{2C} \\ \vdots & \ddots & \ddots & \vdots \\ \boldsymbol{\Lambda}_{C1} & \boldsymbol{\Lambda}_{C2} & \cdots & \boldsymbol{\Lambda}_{CC} \end{bmatrix}$. The convergence of the control filters is guaranteed as long as the step size satisfies $\rho(\mathbf{I}_{CL} - \mu_{\mathbf{w}} \boldsymbol{\Lambda}) < 1$, where $\rho(\bullet)$ is the spectral radius [8].

IV. Simulation Validation

A. Computational Complexity and System Configuration

Table I presents the average number of multiplications per sample for the control filter, secondary path modeling filter, and primary path modeling filter across both time and frequency domains in the FDSCM algorithm.

TABLE I. The average number of multiplications per sample for FDSCM algorithm.

	Time domain	Frequency domain
Control filter	$CR(L+1)$	$CR(20M+4) + 2(CR + M + R)\log_2(2L)$
Secondary path modeling filter	$MC(L+1)$	$C(ML+12M+4) + 2(MC + M + C)\log_2(2L)$
Primary path modeling filter	$MR(L+1)$	$R(ML+12M+4) + 2MR\log_2(2L)$

A 1 × 2 × 2 multichannel ANC system was established in a medium-sized meeting room with dimensions of 7.7 m × 5.7 m × 3.3 m. The overall experimental configuration is illustrated in Fig. 3. Initially, microphones 1 and 2 capture the error signals (defined as scenario 1), while microphones 3 and 4 simulate an abrupt change in the system, leading to variations in both the primary and secondary paths (defined as scenario 2). Subsequent simulations involve setting each filter length to $I = J = K = 512$ and the FFT length to $2L = 1024$. In this case, the FDSCM algorithm requires an average of 7,628 multiplications per sample, whereas the Hu's algorithm [11] necessitates 6,308,872. The computational burden of the FDSCM algorithm incurs only 0.12% of that of the Hu's algorithm, indicating a substantial reduction in computational burden.

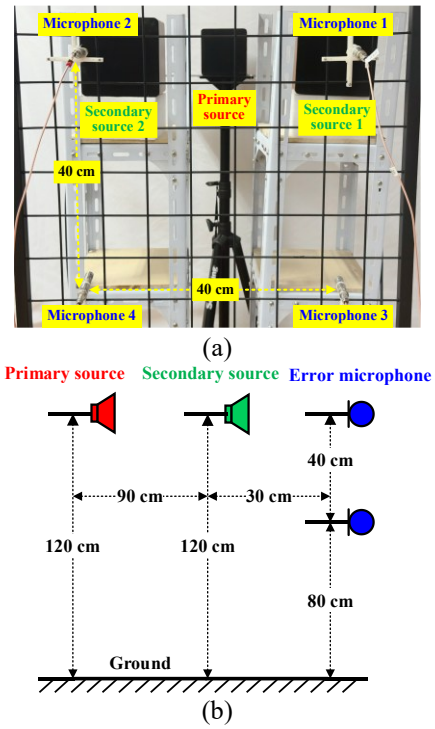

Fig. 3. System configuration with (a) front view photo and (b) side view schematic diagram.

B. *Modeling and Control Results with Measured Acoustic Paths*

The secondary and primary paths are measured using the finite impulse response (FIR) filters at a sampling rate of 2 kHz. The reference signal is an AR(1) process with coefficients (1, −0.8). Uncorrelated system noise with a signal-to-noise ratio (SNR) of 45 dB is introduced at the error microphones to simulate a practical environment. The first and last coefficients of the control filters are initialized as 0.1, while the others are set to zeros. The coefficients of the path modeling filters are initialized as all zeros. Optimal step sizes determined through a trial-and-error approach are employed in the TDNFxLMS algorithm (without path modeling) [8], the Hu's algorithm [11] and the FDSCM algorithm, ensuring the best convergence performance. Define the normalized mean square deviation (NMSD) of the modeling secondary and primary paths as

$$\begin{aligned} \mathrm{NMSD_s} &= \frac{1}{MC}\sum_{m=1}^{M}\sum_{c=1}^{C} 10\log_{10}\left(\left\|\mathbf{s}_{mc}-\hat{\mathbf{s}}_{mc}\right\|^2 / \left\|\mathbf{s}_{mc}\right\|^2\right), \\ \mathrm{NMSD_p} &= \frac{1}{M}\sum_{m=1}^{M} 10\log_{10}\left(\left\|\mathbf{p}_{m}-\hat{\mathbf{p}}_{m}\right\|^2 / \left\|\mathbf{p}_{m}\right\|^2\right), \end{aligned} \tag{29}$$

to evaluate the modeling accuracy.

Under scenario 1, the modeling results for the secondary and primary paths, illustrated in Fig. 4, demonstrate sufficient accuracy, characterized by low $\mathrm{NMSD_s}$ and $\mathrm{NMSD_p}$ values of −44.1 dB and −43.8 dB, respectively.

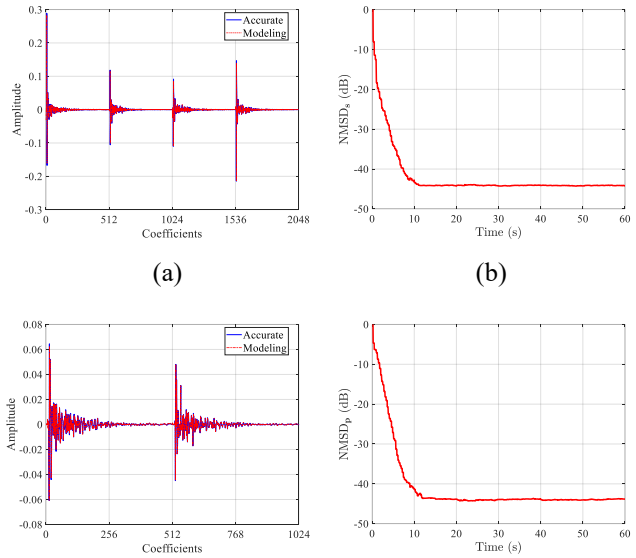

Fig. 4. Modeling results for (a) the coefficients and (b) $\mathrm{NMSD_s}$ of secondary paths, and (c) the coefficients and (d) $\mathrm{NMSD_p}$ of primary paths under scenario 1.

Fig. 5 depicts the average sound pressure level (SPL) curves for microphones 1 and 2 employing the TDNFxLMS algorithm, the Hu's algorithm and the FDSCM algorithm, together with Wiener solution [17] for comparison. Due to its employment of exact secondary paths, the TDNFxLMS algorithm demonstrates a faster convergence speed compared to Hu's algorithm and FDSCM algorithm, both of which necessitate path modeling. The FDSCM algorithm updates the filter block-wise, leading to slightly slower early-stage convergence compared to Hu's point-wise approach. However, the frequency-domain step-size normalizations in (12) and (13) significantly accelerate the convergence rate of the FDSCM algorithm, enabling it to achieve the Wiener solution in approximately 25 s.

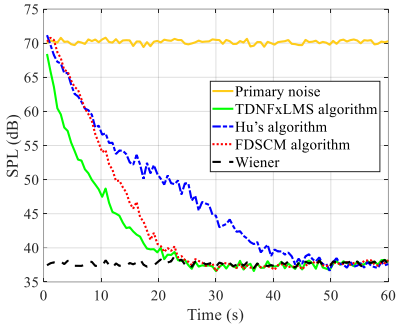

Fig. 5. Average SPL curves under scenario 1.

To simulate a dynamic acoustic environment, microphones 1 and 2 (scenario 1) are switched to microphones 3 and 4 (scenario 2) at 40 s. Fig. 6 presents the modeling results following the transition to scenario 2, reporting $\mathrm{NMSD_s}$ and $\mathrm{NMSD_p}$ values of −42.9 dB and −41.8 dB, respectively, demonstrating that FDSCM algorithm effectively tracks system variations.

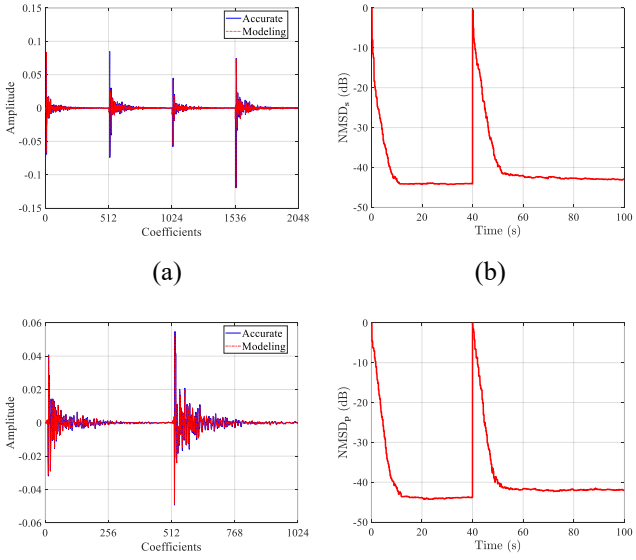

Fig. 6. Modeling results for (a) the coefficients and (b) $\mathrm{NMSD_s}$ of secondary paths, and (c) the coefficients and (d) $\mathrm{NMSD_p}$ of primary paths under scenario 2.

Under dynamic conditions, the average SPL curves for the three algorithms are presented in Fig. 7. The initial 40 s correspond to the average SPL at microphones 1 and 2, while the subsequent period from 40 to 100 s pertains to microphones 3 and 4. The TDNFxLMS algorithm, lacking path modeling capabilities, diverges rapidly after the abrupt path change. In contrast, the FDSCM algorithm achieves the fastest convergence to the Wiener solution at approximately 80 s, while maintaining significantly lower computational complexity compared to the Hu's algorithm.

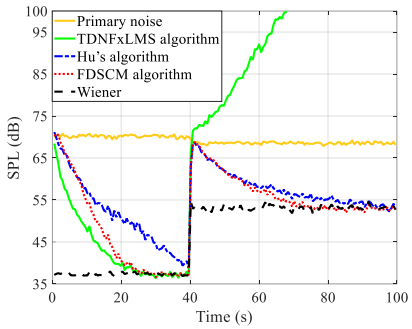

Fig. 7. Average SPL curves under dynamic conditions transitioning from scenario 1 to scenario 2.

V. Conclusions

This paper presents an efficient frequency-domain online modeling of multiple secondary paths without auxiliary noise for ANC. The control process of the algorithm is synchronized with the modeling process of the secondary and primary paths. All the filters are updated in frequency domain to alleviate computational burden, and normalized step sizes are employed to accelerate the convergence speed. Simulations under steady and dynamic conditions confirm its fast convergence speed and robustness, rendering it suitable for real-time multichannel ANC applications with time-varying acoustic environments.

VI. Acknowledgment

This research is supported by the Postgraduate Research & Practice Innovation Program of Jiangsu Province (Grants No. KYCX25_0166 and KYCX25_0160).

References

[1] S. Lian *et al.*, "An online decoupling-whitening frequency domain filtered-error least mean square algorithm for active road noise control," *The Journal of the Acoustical Society of America,* vol. 156, no. 2, pp. 1413-1424, 2024.

[2] T. Li, S. Lian, S. Zhao, J. Lu, and I. S. Burnett, "Distributed active noise control based on an augmented diffusion FxLMS algorithm," *IEEE/ACM Transactions on Audio, Speech, and Language Processing,* vol. 31, pp. 1449-1463, 2023.

[3] I. T. Ardekani and W. H. Abdulla, "Effects of imperfect secondary path modeling on adaptive active noise control systems," *IEEE Transactions on Control Systems Technology,* vol. 20, no. 5, pp. 1252-1262, 2011.

[4] J. Y. Oh, H. W. Jung, M. H. Lee, K. H. Lee, and Y. J. Kang, "Enhancing active noise control of road noise using deep neural network to update secondary path estimate in real time," *Mechanical Systems and Signal Processing,* vol. 206, p. 110940, 2024.

[5] Z. Jia, X. Zheng, Q. Zhou, Z. Hao, and Y. Qiu, "A hybrid active noise control system for the attenuation of road noise inside a vehicle cabin," *Sensors,* vol. 20, no. 24, p. 7190, 2020.

[6] D. W. Kim, J. Hur, and P. Park, "Two-stage active noise control with online secondary-path filter based on an adapted scheduled-stepsize NLMS algorithm," *Applied Acoustics,* vol. 158, p. 107031, 2020.

[7] S. Pradhan and X. Qiu, "A 5-stage active control method with online secondary path modelling using decorrelated control signal," *Applied Acoustics,* vol. 164, p. 107252, 2020.

[8] S. Elliott, *Signal processing for active control*. London, UK: Elsevier, 2000.

[9] C. Cheng, Z. Liu, W. Chen, X. Li, W. Liao, and C. Lu, "A multi-channel active noise control system using deep learning-based method to estimate secondary path and normalized-clustered control strategy for vehicle interior engine noise," *Applied Acoustics,* vol. 228, p. 110263, 2025.

[10] S. Lian *et al.*, "Frequency domain online secondary path modelling for active noise control without auxiliary noise," in *INTER-NOISE and NOISE-CON Congress and Conference Proceedings*. Institute of Noise Control Engineering, 2023, vol. 268, no. 5, pp. 3041-3049.

[11] M. Hu, J. Xue, and J. Lu, "Online multi-channel secondary path modeling in active noise control without auxiliary noise," *The Journal of the Acoustical Society of America,* vol. 146, no. 4, pp. 2590-2595, 2019.

[12] B. Farhang-Boroujeny, *Adaptive filters: theory and applications*. John Wiley & Sons, 2013.

[13] J. Lu, K. Chen, and X. Qiu, "Convergence analysis of the modified frequency-domain block LMS algorithm with guaranteed optimal steady state performance," *Signal Processing,* vol. 132, pp. 165-169, 2017.

[14] S. Lian, T. Li, S. Sun, S. Wang, and J. Lu, "A computational-efficient adaptive algorithm based on frequency point selection in multichannel active noise control systems," *Mechanical Systems and Signal Processing,* vol. 238, p. 113176, 2025.

[15] F. Yang, Y. Cao, M. Wu, F. Albu, and J. Yang, "Frequency-domain filtered-x LMS algorithms for active noise control: A review and new insights," *Applied Sciences,* vol. 8, no. 11, p. 2313, 2018.

[16] Y. Zhao, S. Chen, Z. Zhou, Z. Xu, and J. Jia, "A modified feedforward-feedback time-frequency domain hybrid algorithm for multichannel active road noise control system," *Applied Acoustics,* vol. 226, p. 110189, 2024.

[17] S. J. Elliott, "Optimal controllers and adaptive controllers for multichannel feedforward control of stochastic disturbances," *IEEE Transactions on Signal Processing,* vol. 48, no. 4, pp. 1053-1060, 2000.